NUMERICAL STUDY OF AN ANISOTROPICALLY SUPPORTED ROTOR WITH PARAMETRIC EXCITATION

(Date received: 7.12.2007)

Chih Feng Lee[1], Yee Wei Tan[2] and Janusz M. Krodkiewski[3]
[1]Department of Mechanical and Manufacturing Engineering, University of Melbourne
Parkville, Victoria 3010, Australia.
Email: [1]c.lee33@pgrad.unimelb.edu.au

ABSTRACT

Anisotropic structures, e.g. oil journal bearings are often employed as supporting structure for rotating machineries. Moreover, cross-section of rotating element is often non-symmetrical due to various practical reasons. This paper investigates the dynamics of a parametrically excited rotor-support system. The mathematical model of a rotor supported by an anisotropic structure in the middle and supported rigidly at the far-ends is devised. Stability analysis in the rotating speed domain is demonstrated using two numerical approaches based on Runge–Kutta method and Floquet Theory. The performance of these two methods in terms of computational cost and accuracy is compared. In addition, the influence of cross-coefficient stiffness and damping of the anisotropic support on the unstable region is discussed.

Keywords: *Anisotropic Support, Mechanical Vibrations, Rotor, Stability*

1.0 INTRODUCTION

Rotors are the rotating parts of machines. They are widely found in machineries of various sizes, *e.g.* steam turbines, centrifugal compressors, electric motors, pumps and fans. In most applications, the cross sections of rotors are not perfectly symmetrical along its two principal axes. This is due to various practical reasons, for instance, the rotor of an electric motor has slots for coil assembly and shafts are often equipped with keyways. Unsymmetrical cross section of rotor induces difference in stiffness along the two orthogonal directions.

Supporting structures of rotating machineries are often found to be anisotropic. This can be induced by using materials of non-homogenous composition such as wood, polymer laminates and fibre reinforced plastics. Moreover, irregular and unsymmetrical cross section of supporting structure leads to anisotropy. Besides, anisotropy is resulted from interaction with fluid, *e.g.* in the case of oil journal bearings which is commonly employed in turbo-machineries. The oil field in the journal bearings behaves in a nonlinear and anisotropic fashion.

Support structure can be categorised into isotropic and anisotropic support. Generally, for a two-degree-of-freedom support, the stiffness matrix along the principle axes can be represented by

$$\mathrm{K} = \begin{pmatrix} K_x & K_{xy} \\ K_{yx} & K_y \end{pmatrix} \tag{1}$$

For an isotropic support, the diagonal stiffness terms are identical, *i.e.* $K_x = K_y$ and the cross-coefficient stiffness terms are zero, *i.e.* $K_{xy} = K_{yx} = 0$. On the other hand, for an anisotropic support, the cross-coefficient stiffness terms are not identical, *i.e.* $K_x \neq K_y$. A special case for anisotropic support is orthotropic support, where $K_x \neq K_y$ and $K_{xy} = K_{yx} = 0$. The influence of diagonal stiffness terms K_x and K_y on resonance frequency is well-defined and widely studied [10]. However, the influence of cross-coefficient stiffness on resonance frequency has particular peculiarity, and will be focused in this paper.

Various studies on the influence of support anisotropy on the motion of asymmetric shaft have been done previously. Ota and Mizutani [7] investigated the influence of support stiffness on a system supported by two identical anisotropic bearings at the far-ends of rotor. A lumped mass model with a journal in the middle of the rotor is considered. However, the influence of support damping was not investigated in this paper. Rajilingham et al. [9] extended the investigation by exploring the influence of support damping characteristics. Lee *et al.* [5] approached the problem with Floquet theory and coordinate transformation method. In addition, Ganesan [2] looked into a problem with slightly different configuration. Instead of having two anisotropic support structures, the rotor is supported by an anisotropic structure in the middle and rigidly supported at the far-ends. He also studied the system stability in slowly varying rotation speed.

Parszeski *et al.* [8] investigated the problem with continuous shaft model. They showed that the problem of parametric instability of a rotor-support system could be solved when receptances of rotor-support structure are known. The receptances were obtained using rigid finite element method. Iwatsubo *et al.* [3] approached the problem with continuous shaft using Galerkin's method while Kang *et al.* [4] used transfer matrix method.

In this paper, a lumped mass model with a journal in the middle of the rotor is adopted. The rotor is supported anisotropically in the middle and supported rigidly at the far-ends. Stability analysis of free vibration is obtained by two numerical approaches based

on Runge–Kutta method and Floquet Theory. The former method numerically integrates the equation of motion, while the latter method takes account of the periodicity nature of parametric excitation. Based on Floquet Theory, the solution of periodically perturbed system can be sought using Hill's infinite determinant. By reducing the order of Hill's infinite determinant into smaller matrix, approximating solution for the critical speed region can be found. However, the size of concatenation is not well-defined and its resultant accuracy is questionable. Therefore, in order to verify the solution of Hill's infinite determinant, it is compared with the solution obtained using Runge-Kutta method.

The focus of this paper is on: (a) comparing the computational cost and accuracy of reduced order Hill's determinant and Runge-Kutta method; (b) investigating the influence of cross-coefficient stiffness terms and (c) support damping on unstable speed regions. The remainder of this paper is organised as follows. Section 2 presents the mathematical model of a rotor system with anisotropic support and parametric excitation. Classification of unstable dynamics will be discussed here. Section 3 illustrates two approaches for identification of stable and unstable operating speed regions, namely Runge-Kutta method and Hill's determinant. Section 4 compares the computational cost and accuracy of these two approaches. Section 5 discusses the influence of cross-coefficient stiffness and damping on unstable regions. Section 6 offers some concluding remarks.

2.0 PROBLEM DEFINITION

In this section, the model of rotor-bearing system is introduced, followed by categorisation of unstable dynamic motion.

2.1 Mathematical model

A model of multi-bearing rotor system is devised in order to analyse the influence of support anisotropy (see Figure 1). The rotor is a massless shaft with unsymmetrical cross-section. It is rigidly supported at both ends by two rolling element bearings with isotropic supports. Between the two supports, a journal of mass m is attached and it is supported by an anisotropic structure. Moreover, the residual unbalance of the journal is denoted by μ. The rotor rotates with constant angular speed Ω.

In the model, coordinate system xyz is stationary, while coordinate system $x_R y_R z_R$ is rotating with the shaft. Without loss of generality, the stationary axes xy coincide with the principal axes of the anisotropic support. Reaction force of shaft acting on journal, R is dependent upon the stiffness of shaft. The components of shaft stiffness along the rotating coordinates x_R and y_R are k_x and k_y respectively. If refereed to the rotating coordinates, the components of reaction force are

$$R_{xR} = k_x x_R,$$

$$R_{yR} = k_y Y_R \tag{2}$$

Likewise, the reaction force of the support on journal is dependent on its stiffness and damping. If refereed to the stationary coordinates, the components of the supporting force are

$$S_x = K_x x + K_{xy} y + C_x x\,,$$

$$S_y = K_{xy} x + K_y y + C_y y\,, \tag{3}$$

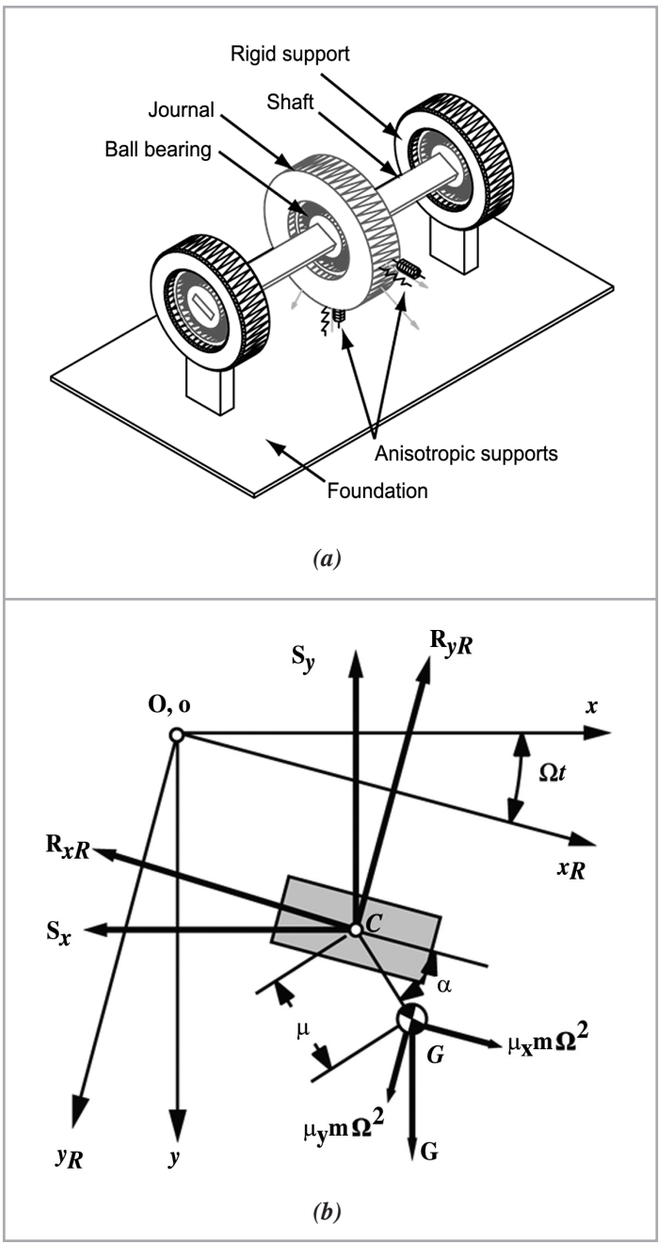

Figure 1: (a) Isometric view of the rotor-bearing-foundation system. (b) Cross-sectional view of forces acting on the rotor

where K and C are stiffness and damping coefficients of the anisotropic support.

Due to external factors such as friction, there exists external damping acting to the journal. The external damping coefficient is represented by c. In addition, due to residual unbalance in the journal, unbalance force exits, and its x and y components are denoted by q_x and q_y respectively. By applying Newton's law to the journal, the equations of motion in x and y directions are

$$m\ddot{x} + (C_x + c)\dot{x} + k_x x_R \cos(\Omega t) - k_y y_R \sin(\Omega t) + K_x x + K_{xy} y = q_x\,,$$

$$m\ddot{y} + (C_y + c)\dot{y} + k_x x_R \sin(\Omega t) + k_y y_R \cos(\Omega t) - K_{xy} x + K_y y =$$

$$G + q_y\,, \tag{4}$$

where G is gravitational force.

By referring to Figure 1, the relationships between rotating coordinate system $x_R y_R$ and stationary coordinate system xy are found to be

$$x_R = x\cos(\Omega t) + y\sin(\Omega t),$$
$$y_R = -x\sin(\Omega t) + y\cos(\Omega t), \tag{5}$$

Hence, introduction of (5) into (4) yields

$$m\ddot{x} + (C_x + c)\dot{x} + \frac{1}{2}(k_x + k_y)x + \frac{1}{2}(k_x - k_y)y\sin(2\Omega t) + \frac{1}{2}(k_x - k_y)x\cos(2\Omega t) + K_x x + K_{xy} y = q_x,$$
$$m\ddot{y} + (C_y + c)\dot{y} + \frac{1}{2}(k_x + k_y)y - \frac{1}{2}(k_x - k_y)y\cos(2\Omega t) + \frac{1}{2}(k_x - k_y)x\sin(2\Omega t) + K_y y - K_{xy} x = G + q_y, \tag{6}$$

To further analyse the problem, the following notations are introduced, namely mean and difference of diagonal stiffness terms, *i.e.* k_0 and Δk respectively.

$$k_0 = \frac{1}{2}(k_x + k_y), \quad \Delta k = \frac{1}{2}(k_x - k_y) \tag{7}$$

Then, introduction of (7) into (6) gives

$$m\ddot{x} + (C_x + c)\dot{x} + k_0 x + \Delta k y\sin(2\Omega t) + \Delta k x\cos(2\Omega t) + K_x x + K_{xy} y = q_x,$$
$$m\ddot{y} + (C_x + c)\dot{y} + k_0 y - \Delta k y\cos(2\Omega t) + \Delta k x\sin(2\Omega t) + K_y y - K_{xy} x = G + q_y. \tag{8}$$

The components of residual unbalanced force in x and y directions are

$$q_x = \mu_x m\Omega^2\cos(\Omega t) - \mu_y m\Omega^2\sin(\Omega t),$$
$$q_y = \mu_x m\Omega^2\sin(\Omega t) + \mu_y m\Omega^2\cos(\Omega t), \tag{9}$$

where

$$\mu_x = \mu\cos(\alpha),\ \mu_y = \mu\sin(\alpha) \tag{10}$$

Equation (8) can be arranged into the following matrix representation

$$\begin{pmatrix} m & 0 \\ 0 & m \end{pmatrix}\begin{pmatrix} \ddot{x} \\ \ddot{y} \end{pmatrix} + \begin{pmatrix} Cx + c & 0 \\ 0 & Cx + c \end{pmatrix}\begin{pmatrix} \dot{x} \\ \dot{y} \end{pmatrix} + \begin{pmatrix} K_x & K_{xy} \\ -K_{xy} & K_y \end{pmatrix}\begin{pmatrix} x \\ y \end{pmatrix} + \left\{\begin{pmatrix} k_0 & 0 \\ 0 & k_0 \end{pmatrix} + \begin{pmatrix} 0 & \Delta k \\ \Delta k & 0 \end{pmatrix}\sin(2\Omega t) + \begin{pmatrix} \Delta k & 0 \\ 0 & -\Delta k \end{pmatrix}\cos(2\Omega t)\right\}\begin{pmatrix} x \\ y \end{pmatrix} = \begin{pmatrix} 0 \\ G \end{pmatrix} + \begin{pmatrix} q_x \\ q_y \end{pmatrix}. \tag{11}$$

By introducing matrix notation

$$\boldsymbol{z} = \begin{pmatrix} x \\ y \end{pmatrix}, \tag{12}$$

and defining the corresponding matrices, Equation (11) is written in a compact form

$$\boldsymbol{M}\ddot{\boldsymbol{z}} + \boldsymbol{C}\dot{\boldsymbol{z}} + \boldsymbol{K}\boldsymbol{z} + (\boldsymbol{k}_0 + \Delta\boldsymbol{k}_s\sin(2\Omega\boldsymbol{t}) + \Delta\boldsymbol{k}_c\cos(2\Omega\boldsymbol{t}))\boldsymbol{z} = \boldsymbol{Q} + \boldsymbol{q}. \tag{13}$$

Then, using Euler formulae

$$\sin(2\Omega t) = \frac{e^{i2\Omega t} - e^{-i2\Omega t}}{2i}$$
$$\cos(2\Omega t) = \frac{e^{i2\Omega t} + e^{-i2\Omega t}}{2i} \tag{14}$$

the equation of motion is arranged into the following expression

$$\boldsymbol{M}\ddot{\boldsymbol{z}} + \boldsymbol{C}\dot{\boldsymbol{z}} + \boldsymbol{K}\boldsymbol{z} + \left(\boldsymbol{k}_0 + \frac{1}{2}(\Delta\boldsymbol{k}_c + \boldsymbol{i}\Delta\boldsymbol{k}_s)\boldsymbol{e}^{i2\Omega t} + \frac{1}{2}(\Delta\boldsymbol{k}_c - \boldsymbol{i}\Delta\boldsymbol{k}_s)\boldsymbol{e}^{-i2\Omega t}\right)\boldsymbol{z} = \boldsymbol{Q} + \boldsymbol{q}. \tag{15}$$

To analyse the influence of anisotropic support and non-symmetrical shaft on dynamic motion, the investigation is concentrated on dynamic motion free from any impressed force – the free vibration case. The equation of motion for free vibration is the homogeneous equation of (15), *i.e.*

$$\boldsymbol{M}\ddot{\boldsymbol{z}} + \boldsymbol{C}\dot{\boldsymbol{z}} + \boldsymbol{K}\boldsymbol{z} + \left(\boldsymbol{k}_0 + \frac{1}{2}(\Delta\boldsymbol{k}_c + \boldsymbol{i}\Delta\boldsymbol{k}_s)\boldsymbol{e}^{i2\Omega t} + \frac{1}{2}(\Delta\boldsymbol{k}_c - \boldsymbol{i}\Delta\boldsymbol{k}_s)\boldsymbol{e}^{-i2\Omega t}\right)\boldsymbol{z} = 0. \tag{16}$$

2.2 Classification of unstable regions

If there is no parametric excitation, *i.e.* $\Delta k = 0$, the system possesses two natural frequencies:

$$\omega_1 = \sqrt{\frac{k_0 + k_x}{m}}, \quad \omega_2 = \sqrt{\frac{k_0 + k_y}{m}} \tag{17}$$

With the combined effects of anisotropic supporting structure and parametric vibration, the unstable regions are often found in vicinity of the natural frequencies. The unstable regions associated with only one natural frequency are termed simple instability regions. They can be determined by:

$$\Omega_{nl} = \frac{\omega_n}{l}, \quad l = 1, 2, \ldots\ldots \tag{18}$$

Apart from the simple instability regions, some unstable regions are associated with both of the natural frequencies. They are termed combined instability regions. They can be found in vicinity of:

$$\Omega^{(\pm)}_{nml} = \frac{\omega_n \pm \omega_n}{2l}, \quad l = 1, 2, \ldots\ldots \tag{19}$$

When $l = 1$, the unstable region is called primary instability region; when $l = 2$, it is called secondary instability region.

3.0 METHODS TO DETERMINE STABILITY REGIONS

One of the operation safety concerns of rotating machineries is to avoid operating close to critical speeds. Therefore in the design stage, it is important to identify the critical speed regions. Operating under critical speed yields unstable dynamic motion, where the amplitude of vibration grows exponentially. For complex cases, such as the case expressed in (16), it is very difficult to obtain an exact analytical solution of the critical speed regions. Hence, numerical solution is sought. This section illustrates two numerical methods for determination of stable and unstable operating speed regions. They are based on Runge-Kutta method and Floquet theory.

3.1 Numerical methods for ordinary differential equations

The ordinary differential equation with time derivative, such as equation (16) can be written in the following general form

$$y(t) = \frac{dy(t)}{dt} = f(t, y). \tag{20}$$

Numerical schemes, such as Euler's method, Crank-Nicolson method and Runge-Kutta method are often employed to obtain numerical solutions for ordinary differential equations. Compared among other methods, the forth-order Runge-Kutta method has a few preferred numerical features, *e.g.* it is relatively simpler to code than Crank-Nicolson method, its numerical solution is more stable than Euler method, and it generally has fast evaluation speed. Therefore, the forth-order Runge-Kutta method is chosen in this study.

3.1.1 Runge-Kutta Method

Runge-Kutta methods has the following generalised form [1]

$$y_{i+1} = y_i + \phi(t_i, y_i, h)\, h. \tag{21}$$

where h and $\phi(t_i, y_i, h)$ are called step size and increment function respectively. The increment function can be used as a representative of the slope over interval $(t_i, t_i + h)$ and it differentiates from different orders of Runge-Kutta methods. The general form of the increment function is

$$\phi(t_i, y_i, h) = a_1 k_1 + a_2 k_2 + \ldots + a_n k_n , \tag{22}$$

where the a's are constants and the k's are

$$\begin{aligned}
k_1 &= f(t_i, y_i) \\
k_2 &= f(t_i + p_1 h, y_i + q_{11} k_1 h) \\
k_3 &= f(t_i + p_2 h, y_i + q_{21} k_1 h + q_{22} k_2 h) \\
&\vdots \\
k_n &= f(t_i + p_{n-1} h, y_i + q_{n-1,1} k_1 h + q_{n-1,2} k_2 h + \ldots + q_{n-1,n-1} k_{n-1} h)
\end{aligned} \tag{23}$$

p's and q's are constants.

Various order of Runge-Kutta methods are devised by employing different n's, specified in the increment function. The constants a's, p's and q's are evaluated by employing Taylor series expansion [1]. The most popular Runge-Kutta methods is the forth-order Runge-Kutta scheme, where its classical form has the following increment function [1]

$$\phi_{RK4}(t_i, y_i, h) = \frac{1}{6} k_1 + \frac{1}{3} k_2 + \frac{1}{3} k_3 + \frac{1}{6} k_4 , \tag{24}$$

where

$$\begin{aligned}
k_1 &= f(t_i, y_i) \\
k_2 &= f(t_i + \tfrac{1}{2} h, y_i + \tfrac{1}{2} k_1 h) \\
k_3 &= f(t_i + \tfrac{1}{2} h, y_i + \tfrac{1}{2} k_2 h) \\
k_4 &= f(t_i + h, y_i + k_3 h)
\end{aligned} \tag{25}$$

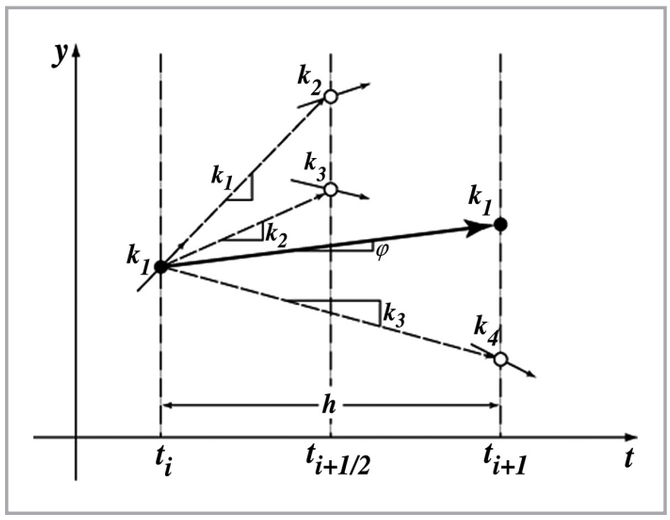

Figure 2: Graphical representation of forth-order Runge-Kutta slope estimation [1]

The step size h determines the accuracy of the solution and the speed of evaluation. Accuracy of the solution increases with the decrease of step size, however, in the expense of slower evaluation speed. Moreover, large step size can induce numerical instability. Therefore, determination of the correct step size is vital.

It is worthwhile to mention that the step size of certain variant of Runge-Kutta methods is varied during evaluation, such as the Runge-Kutta Fehlberg method. There are two notable benefits for using adaptive step size: (a) to avoid numerical instability and (b) to increase the evaluation speed by using the largest possible step size while maintaining the required accuracy tolerance. In particular for Runge-Kutta Fehlberg method, solutions obtained with forth- and firth-order are compared. Difference between the solutions is the estimated numerical truncation error [1]. Consequently, truncation error is used to determine the next step size. The strategy is to decrease the step size if the error is too large and vice-versa.

The following subsection describes the steps required to solve a set of ordinary differential equations, *e.g.* (16) using Runge-Kutta method.

3.1.2 Evaluation of a Second Order Differential Equation

Differential equations that involve one dependent variable are called ordinary differential equations. They are classified by the order of their highest derivative. For example, the highest order of derivative for the equation of motion (16) is two.

Therefore, (16) is a second order ordinary differential equation. In order to solve a set high-order differential equations using forth-order Runge-Kutta method, they are arranged into a set of first-order differential equations, which can be written concisely as

$$\dot{\boldsymbol{y}} = \boldsymbol{A}\boldsymbol{y} + \boldsymbol{B} \tag{26}$$

Equation (16) can be arranged into the form of (26), *i.e.*

$$\begin{pmatrix} \dot{z} \\ \ddot{z} \end{pmatrix} = \begin{bmatrix} 0 & 1 \\ -\boldsymbol{M}^{-1}(\boldsymbol{K}+\boldsymbol{k}_0) & -\boldsymbol{M}^{-1}\{1/2(\Delta\boldsymbol{k}_c + \boldsymbol{i}\Delta\boldsymbol{k}_s)\exp(\boldsymbol{i}2\Omega t) \\ & +1/2(\Delta\boldsymbol{k}_c - \boldsymbol{i}\Delta\boldsymbol{k}_s)\exp(-\boldsymbol{i}2\Omega t)\} \end{bmatrix} \begin{pmatrix} z \\ \dot{z} \end{pmatrix} \tag{27}$$

Henceforth, (27) can be solved using the equations as described in (21), (24) and (25).

Numerous mathematics packages such as Mathematica and MATLAB includes ordinary differential equation solvers. In particular, the results presented in this paper are obtained using MATLAB "ode45" function, which is based upon fifth- and sixth-order Runge-Kutta method with adaptive step size.

3.2 Floquet Theory

The governing differential equation of free vibration equation (16) contains coefficients that are periodic. These periodic coefficients pose excitation to the system, in which the type of excitation is termed parametric excitation. In contrast to the case of external excitation, where resonance only happens when the excitation is close to one of the natural frequencies of the system, resonance in parametric excitations may happen when the frequency of excitation is close to one half of one of the natural frequencies [6].

For systems governed by ordinary differential equations with periodic coefficients, Floquet theory is commonly used as the basis for analysis. According to Floquet theory, these systems has particular solutions of the form [6]

$$z = \exp(\gamma t)\,\varphi(t) \tag{28}$$

where γ is called characteristic exponent or Floquet exponent. It is a complex number, in which its real part is called Lyapunov exponent. $\varphi(t)$ is a periodic function, *i.e.* $\varphi(t) = \varphi(t + T)$, where T is the period of the excitation. From (16), it is noticed that $T = 2\pi/2\Omega = \pi/\Omega$. Expressing $\varphi(t)$ in Fourier series yields

$$\varphi(t) = \sum_{n=-\infty}^{\infty} \exp(i2n\Omega t)\,\varphi_n \tag{29}$$

Therefore, substituting (29) into the particular solution (28) to procure

$$z = \sum_{n=-\infty}^{\infty} \exp(\gamma t + i2n\Omega t)\,\varphi_n \tag{30}$$

It is noted that the solution (28) is unstable if, and stable for in Lyapunov sense. The following subsection illustrates a method for determining the stability boundary.

3.2.1 Hill'S Infinite Determinant

By differentiating (30), we get

$$\dot{z} = \sum_{n=-\infty}^{\infty} \exp(\gamma t + i2n\Omega t)(\gamma + i2n\Omega)\,\varphi_n, \qquad \ddot{z} = \sum_{n=-\infty}^{\infty} \exp(\gamma t + i2n\Omega t)(\gamma + i2n\Omega)^2\,\varphi_n \tag{31}$$

Substituting (30) and (31) into (16) yields

$$\sum_{n=-\infty}^{\infty} \left\{ \left[\boldsymbol{M}(\gamma + i2n\Omega)^2 + \boldsymbol{C}(\gamma + i2n\Omega) + \boldsymbol{K} + \boldsymbol{k}_0 \right] \varphi_n \exp(\gamma t + i2n\Omega t) \right\}$$
$$+ \frac{1}{2}(\Delta\boldsymbol{k}_c + i\Delta\boldsymbol{k}_s) \sum_{n=-\infty}^{\infty} \left\{ (\varphi_n \exp(\gamma t + i(2n+1)\Omega t) \right\}$$
$$+ \frac{1}{2}(\Delta\boldsymbol{k}_c - i\Delta\boldsymbol{k}_s) \sum_{n=-\infty}^{\infty} \left\{ (\varphi_n \exp(\gamma t + i(2n-1)\Omega t) \right\} \tag{32}$$

Equating the coefficients for each of the exponential terms $\exp(\gamma t + i2n\Omega t)$ in (32) to zero, we get the following infinite set of equations, corresponding to φ_m (where $m = -\infty, \ldots, \infty$)

$$\left[\boldsymbol{M}(\gamma + i2n\Omega)^2 + \boldsymbol{C}(\gamma + i2n\Omega) + \boldsymbol{K} + \boldsymbol{k}_0 \right] \varphi_m + \frac{1}{2}(\Delta\boldsymbol{k}_c + i\Delta\boldsymbol{k}_s)\varphi_{m+1}$$
$$+ \frac{1}{2}(\Delta\boldsymbol{k}_c + i\Delta\boldsymbol{k}_s)\varphi_{m+1} = 0 \tag{33}$$

Presenting (33) in matrix notation gives

$$\begin{pmatrix} \ddots & \vdots & \vdots \\ \cdots & \boldsymbol{M}(\gamma - i2\Omega)^2 + \boldsymbol{C}(\gamma - i2\Omega) + \boldsymbol{K} + \boldsymbol{k}_0 & \frac{1}{2}(\Delta\boldsymbol{k}_c + i\Delta\boldsymbol{k}_s) \\ \cdots & \frac{1}{2}(\Delta\boldsymbol{k}_c + i\Delta\boldsymbol{k}_s) & \boldsymbol{M}\gamma^2 + \boldsymbol{C}\gamma + \boldsymbol{K} + \boldsymbol{k}_0 \\ \cdots & 0 & \frac{1}{2}(\Delta\boldsymbol{k}_c + i\Delta\boldsymbol{k}_s) \\ \iddots & \vdots & \vdots \end{pmatrix}$$
$$\begin{pmatrix} \vdots & \iddots \\ 0 & \cdots \\ \frac{1}{2}(\Delta\boldsymbol{k}_c - i\Delta\boldsymbol{k}_s) & \cdots \\ \boldsymbol{M}(\gamma + i2\Omega)^2 + \boldsymbol{C}(\gamma + i2\Omega) + \boldsymbol{K} + \boldsymbol{k}_0 & \cdots \\ \vdots & \ddots \end{pmatrix} \begin{pmatrix} \vdots \\ \varphi_{-1} \\ \varphi_0 \\ \varphi_{+1} \\ \vdots \end{pmatrix} = \begin{pmatrix} \vdots \\ 0 \\ 0 \\ 0 \\ \vdots \end{pmatrix} \tag{34}$$

For a nontrivial solution, the determinant of the coefficient matrix in (34) is equal to zero. Hence, as a function of Floquet exponent and rotation speed, Hill's infinite determinant is

$$\boldsymbol{D}(\gamma, \Omega) = \begin{pmatrix} \ddots & \vdots \\ \cdots & \boldsymbol{M}(\gamma - i2\Omega)^2 + \boldsymbol{C}(\gamma - i2\Omega) + \boldsymbol{K} + \boldsymbol{k}_0 \\ \cdots & \frac{1}{2}(\Delta\boldsymbol{k}_c + i\Delta\boldsymbol{k}_s) \\ \cdots & 0 \\ \iddots & \vdots \end{pmatrix} \tag{35}$$

$$\begin{pmatrix} \vdots & \vdots & \ddots \\ \frac{1}{2}(\Delta \boldsymbol{k}_c + i\Delta \boldsymbol{k}_s) & 0 & \cdots \\ \boldsymbol{M}\gamma^2 + \boldsymbol{C}\gamma + \boldsymbol{K} + \boldsymbol{k}_0 & \frac{1}{2}(\Delta \boldsymbol{k}_c - i\Delta \boldsymbol{k}_s) & \cdots \\ \frac{1}{2}(\Delta \boldsymbol{k}_c + i\Delta \boldsymbol{k}_s) & \boldsymbol{M}(\gamma + i2\Omega)^2 + \boldsymbol{C}(\gamma + i2\Omega) + \boldsymbol{K} + \boldsymbol{k}_0 & \cdots \\ \vdots & \vdots & \ddots \end{pmatrix} = 0$$

As mentioned in the previous subsection, solution (28) is unstable if $\mathrm{Re}(\gamma) > 0$. The transition curves separating stable and unstable motion correspond to $\mathrm{Re}(\gamma) = 0$ [6]. Therefore, (35) is solved as a function of rotation speed and characteristics exponent with only imaginary parts, where $\mathrm{Im}(\gamma) = \mu$. In addition, periodic motion with period 2Ω corresponds to solution at $\gamma = 0$, while 4Ω corresponds to $\gamma = \pm i$. The roots can be plotted as Figure 3, and the stability boundary is located at

$$\mathrm{Re}(D(\mu,\Omega)) = 0 \quad \text{and} \quad \mathrm{Im}\,(D(\mu,\Omega)) = 0 \tag{36}$$

3.2.2 Reduced-Order Hill'S Determinant

When $\Delta k_c + i\Delta k_s$ is small, approximate solution can be obtained by considering the central row and column of (35) [6]. A n^{th} order Hill's reduced order determinant matrix $D(\mu, \Omega)$ has $2n + 1$ rows. For example, a first order Hill's determinant has three rows

$$D_1(\mu, \Omega) = \begin{bmatrix} \boldsymbol{M}(i\mu - i2\Omega)^2 + \boldsymbol{C}(i\mu - i2\Omega) + \boldsymbol{K} + \boldsymbol{k}_0 & \frac{1}{2}(\Delta \boldsymbol{k}_c - i\Delta \boldsymbol{k}_s) & 0 \\ \frac{1}{2}(\Delta \boldsymbol{k}_c + i\Delta \boldsymbol{k}_s) & \boldsymbol{M}(i\mu)^2 + \boldsymbol{C}(i\mu) + \boldsymbol{K} + \boldsymbol{k}_0 & \frac{1}{2}(\Delta \boldsymbol{k}_c - i\Delta \boldsymbol{k}_s) \\ 0 & \frac{1}{2}(\Delta \boldsymbol{k}_c + i\Delta \boldsymbol{k}_s) & \boldsymbol{M}(i\mu + i2\Omega)^2 + \boldsymbol{C}(i\mu + i2\Omega) + \boldsymbol{K} + \boldsymbol{k}_0 \end{bmatrix} \tag{37}$$

To obtain a better approximation, higher-order determinant has to be considered. It is generally unclear what order of determinant has to be considered in order to obtain a valid solution. Therefore, the solution of different orders will be compared and discussed in the following section.

4.0 COMPUTATIONAL ISSUES

In the previous section, it is shown that the stable region can be obtained using Runge-Kutta method and reduced order of Hill's infinite determinant. This section assesses the accuracy and evaluation time of both methods quantitatively.

To study the computing requirement for different orders of Hill's determinant, the computational grid size is fixed as 0.05 [rad/s], and computing time is recorded. It is found that lower computing requirement is required by reducing the order of Hill's determinant (see Table 1). Moreover, percentage increase in computing time diminishes with higher order. To identify the accuracy of solution of the reduced order determinant, it is compared with the solution obtained using Runge-Kutta method, and is tabulated in Table 2. Unstable regions in the rotating speed domain from 0–40 [rad/s] are identified and classified into primary and secondary simple or combined instability regions. Numerical values of the instability boundaries obtained from reduced order of Hill's determinant and Runge-Kutta method are compared, and their percentage differences are calculated. It is observed that:

(i) By increasing the order of Hill's determinant, new unstable regions can be found. In this example, the boundaries of secondary instability region are not revealed by the first-order Hill's determinant.

(ii) By increasing the order of Hill's determinant, better accuracy could be obtained. However, the improvement of accuracy is very minor (approximately 1%) for order more than two.

(iii) Longer computation time is required for higher order Hill's determinant.

(vi) Locating stability boundary is more efficient using Hill's determinant. Estimated evaluation time using Runge-Kutta method is 6400 [s], and 78 [s] for second order Hill's determinant (0.05 [rad/s] accuracy using a Pentium 4 3.0 GHz machine).

Table 1: Evaluation time for reduced order Hill's determinant

Order	Evaluation Time [s]	Time Increase [%]
0	29	–
1	78	169
2	125	60
3	173	38

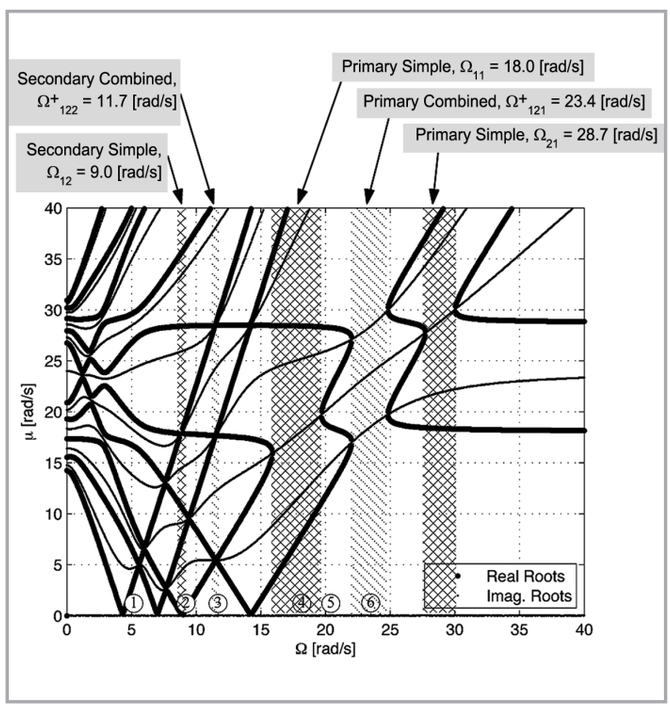

Figure 3: Whirl speed chart calculated using 2nd order Hill's determinant for system supported by orthotropic structure with small damping. The unstable region is hatched

Table 2: Comparison of stability boundaries obtained using different orders of Hill's determinant and Runge-Kutta method

	Secondary Simple		Secondary Combined		Primary Simple		Primary Combined		Primary Simple	
	lower	upper	lower	upper	lower	upper	lower	upper	lower	upper
Runge-Kutta	8.84	8.99	11.49	11.55	15.91	19.67	22.04	24.83	27.74	30.02
Order 1	-	-	-	-	15.84	19.62	22.01	24.82	27.72	30.02
Order 2	8.74	8.90	11.48	11.56	15.90	19.68	22.04	24.83	27.73	30.02
Order 3	8.84	8.99	11.48	11.56	15.90	19.68	22.04	24.83	27.73	30.02
(% diff.) Order 1	-	-	-	-	0.44%	0.25%	0.14%	0.04%	0.07%	0.00%
(% diff.) Order 2	1.13%	1.00%	0.09%	0.09%	0.06%	0.05%	0.00%	0.00%	0.04%	0.00%
(% diff.) Order 3	0.00%	0.00%	0.09%	0.09%	0.06%	0.05%	0.00%	0.00%	0.04%	0.00%

5.0 INFLUENCE OF ANISOTROPIC SUPPORTING STRUCTURE

This section discusses the influence of cross-coefficient stiffness of anisotropic support on the stability region in rotating speed domain. In the following analysis, anisotropic support is categorised into two cases, *i.e*. orthotropic structure and non-orthotropic structure.

5.1 Case $K_{xy} = K_{yx} = 0$ (Orthotropic Structure)

Orthotropic support is a special case of anisotropic support, when the cross-coefficient stiffness terms K_{xy} and K_{yx} are zero. Orthotropic supporting structures include supporting structure with unsymmetrical dimension in the two principal axes and supporting structure constructed with laminating materials, such as wood, polymer laminates and fibre reinforced plastics.

In this subsection, numerical simulation of two cases will be discussed. First, a system with orthotropic support and small damping will be discussed, followed by the same system with large damping.

The simulation parameters for parametric excited system supported with orthotropic structure with small damping are tabulated in Table 3 and the rotating speed associated with simple and combined instability regions are tabulated in Table 4. According to numerical experiments, the unstable regions in the rotating speed domain are found in vicinity of simple and positive combined critical speeds Ω_{nl} and Ω^{+}_{nml} . However, unstable region associated with the negative combined critical speed Ω^{-}_{nml} does not exist. Moreover, it is noticed that the largest unstable region is associated with the primary unstable region. Unstable regions of higher order are usually smaller and are likely to diminish due to the existence of damping.

Spectrum analysis of time history shows that there is only one frequency associated with simple unstable region. On the other hand, there are at least two frequencies associated with the combined unstable regions. The associated frequencies are found to be the natural frequencies of the non-parametrically excited case, as defined in (17). In addition, in the stable regions, the spectrum contains various frequencies, where some of them include the simple and combined critical speeds, as defined in (18) and (19) (see Figures 3 and 4).

Table 3: Simulated system parameters for orthotropic support structure with small damping

Parameters	Values	Parameters	Values
m	50 kg	K_{xy}	0 N/m
k_o	11250 N/m	c	20 N.s/m
Δk	6750 N/m	C_x	0 N.s/m
K_x	5000 N/m	C_y	0 N.s/m
K_y	30000 N/m		

Table 4: Angular speed associated with simple and combined instability regions

Simple	Values [rad/s]	Combined	Values [rad/s]
Ω_{11}	18.0	$\Omega^{(+)}_{121}$	23.35
Ω_{21}	28.7	$\Omega^{(-)}_{121}$	5.35
Ω_{12}	9.0	$\Omega^{(+)}_{122}$	11.68
Ω_{22}	14.4	$\Omega^{(-)}_{122}$	2.68
Ω_{13}	6.0	$\Omega^{(+)}_{123}$	7.78
Ω_{23}	9.6	$\Omega^{(-)}_{123}$	1.78

Unstable region diminishes as damping increases. This is shown in the simulation with parameters tabulated in Table 5. Figure 5 shows that when damping is large, unstable regions in the low frequency range (0–40 [rad/s] in this case) vanish, in exception to the primary simple unstable region associated with Ω_{11}. This is because Ω_{11} is associated with the natural frequency in x, and the damping in x is relatively smaller compared to the damping in y.

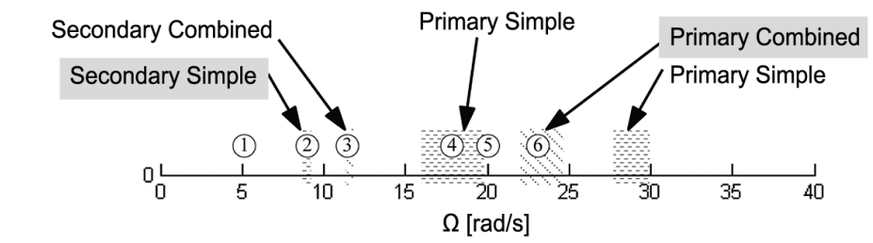

(a)

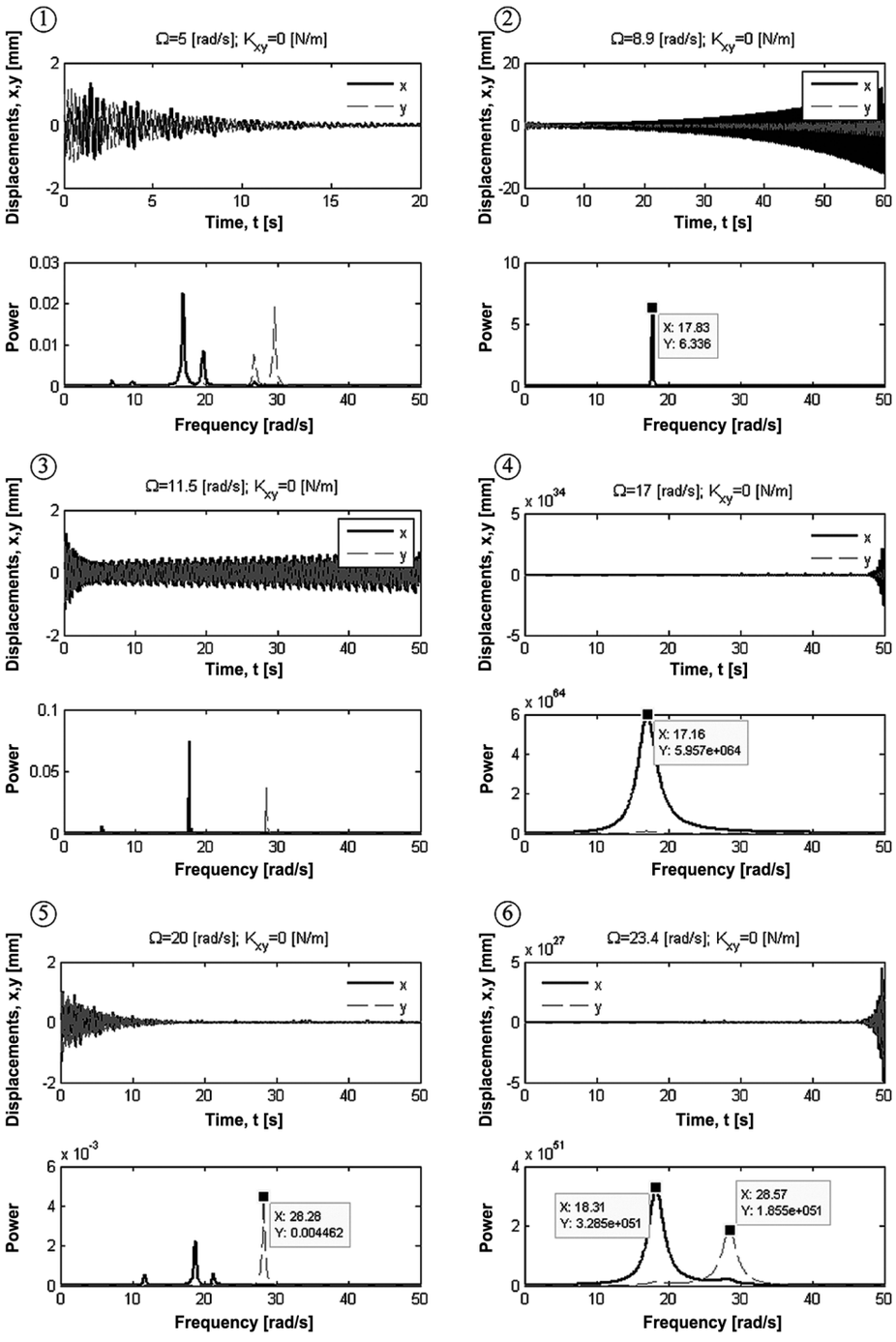

(b)

Figure 4: (a) Unstable regions in rotating speed domain. (b) Time history diagrams and frequency spectrums for various rotating speeds

5.2 Case $K_{xy} = -K_{yx} \neq 0$

The cross-coefficient stiffness terms for non-orthotropic structure are nonzero. This class of anisotropic structure includes oil journal bearings, which are widely used to support rotor in turbomachineries. For anisotropic structure in general, at the principal axes of anisotropy, the cross-coefficient stiffness terms, K_{xy} and K_{yx} have same magnitude with opposite sign.

In this subsection, numerical experiment of a system with large cross-coefficient stiffness and small structural damping (at support) is considered. The system parameters are tabulated in Table 6.

Table 5: Simulated system parameters for orthotropic support structure by large damping

Parameters	Values	Parameters	Values
m	50 kg	K_{xy}	0 N/m
k_o	11250 N/m	c	20 N.s/m
Δk	6750 N/m	C_x	100 N.s/m
K_x	5000 N/m	C_y	500 N.s/m
K_y	30000 N/m		

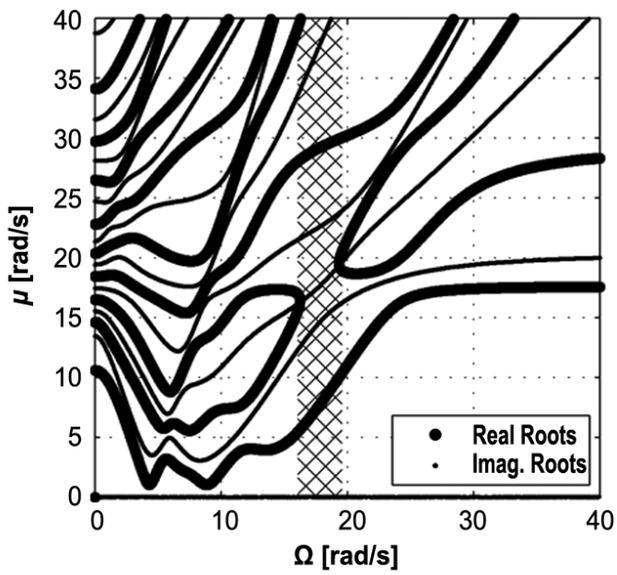

(a)

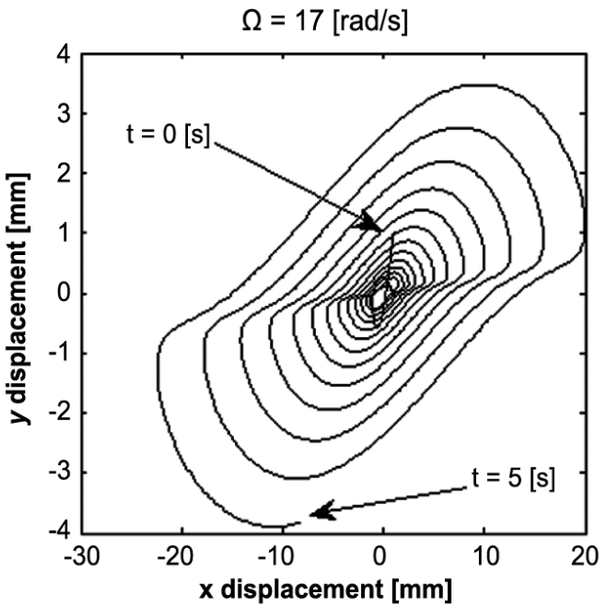

(b)

Figure 5: (a) Whirl speed chart for system supported by orthotropic structure with large damping. The unstable region is hatched. (b) x-y displacement from 0 to 5 seconds for unstable motion

Table 6: Simulated system parameters for anisotropic support structure with small damping

Parameters	Values	Parameters	Values
m	50 kg	K_{xy}	2000 N/m
k_o	11250 N/m	c	20 N.s/m
Δk	6750 N/m	C_x	0 N.s/m
K_x	5000 N/m	C_y	0 N.s/m
K_y	30000 N/m		

Compared with the orthotropic case, strong cross-coefficient stiffness yields new unstable regions (see Figure 6). From simulation, a new secondary simple instability region is found in vicinity of Ω_{21}. Apart, new primary combined instability region is also found in vicinity of $\Omega^{(-)}_{121}$ (see rotating speed range from 5 to 7 [rad/s] in Figure 6). Note that this unstable region associated with negative sign is not found in the orthotropic case. Although $\Omega^{(-)}_{121}$ is very close to the other tertiary speeds (such as Ω_{13} and $\Omega^{(+)}_{123}$), it can be justified that this unstable region is associated with the primary speed. This is because the secondary and tertiary unstable regions are comparatively narrower, and are likely to diminish due to the existence of damping. Conversely, this new found unstable region is large, and is classified as primary combined instability region.

In addition, by observing the location of the stability boundaries, it is found that the boundaries for primary simple instability regions always fall on the line $\mu = \Omega$. Moreover, for secondary simple instability regions, the boundary falls on the line $\mu = 2\Omega$. In fact, for nth order simple instability regions, the stability boundary falls on $\mu = n\Omega$ (see Figure 6).

Figure 7 shows the relationship between unstable region with the magnitude of cross-coefficient stiffness K_{xy} and external damping c. As K_{xy} increases: (a) Overall unstable region increases; (b) Combined instability regions increases; (c) If there are two adjoining unstable regions, they combine as K_{xy} increases. Moreover, unstable regions decrease as external damping increases.

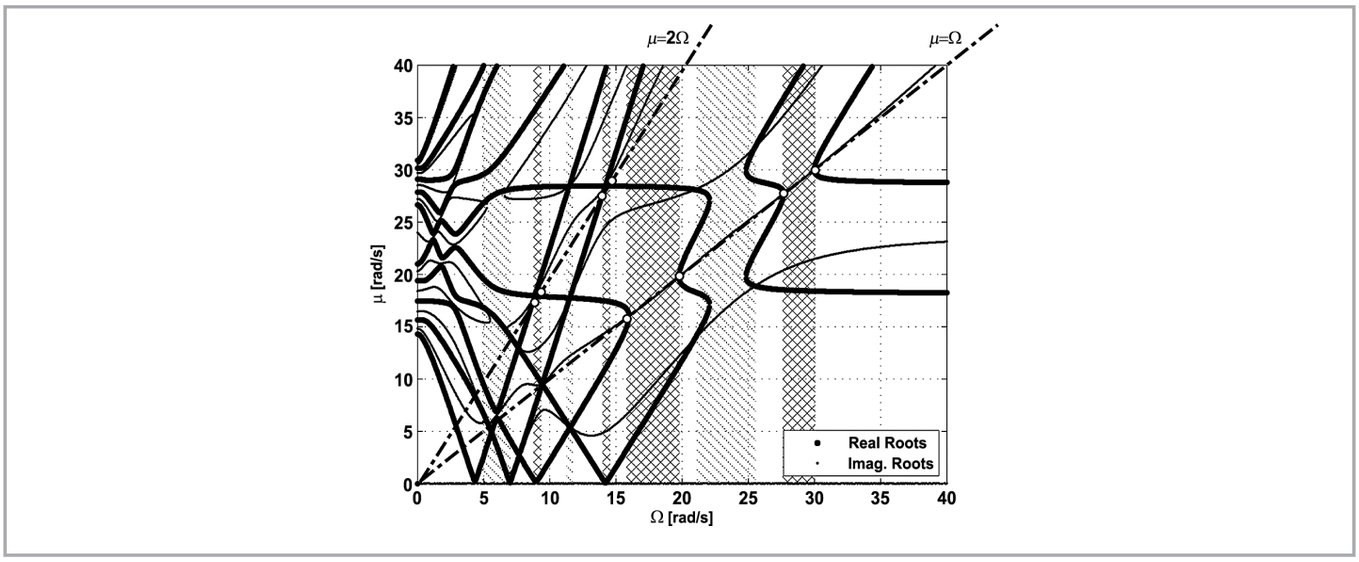

Figure 6: Whirl speed chart for system supported by anisotropic structure with large cross-coefficient stiffness and small damping. The unstable region is hatched

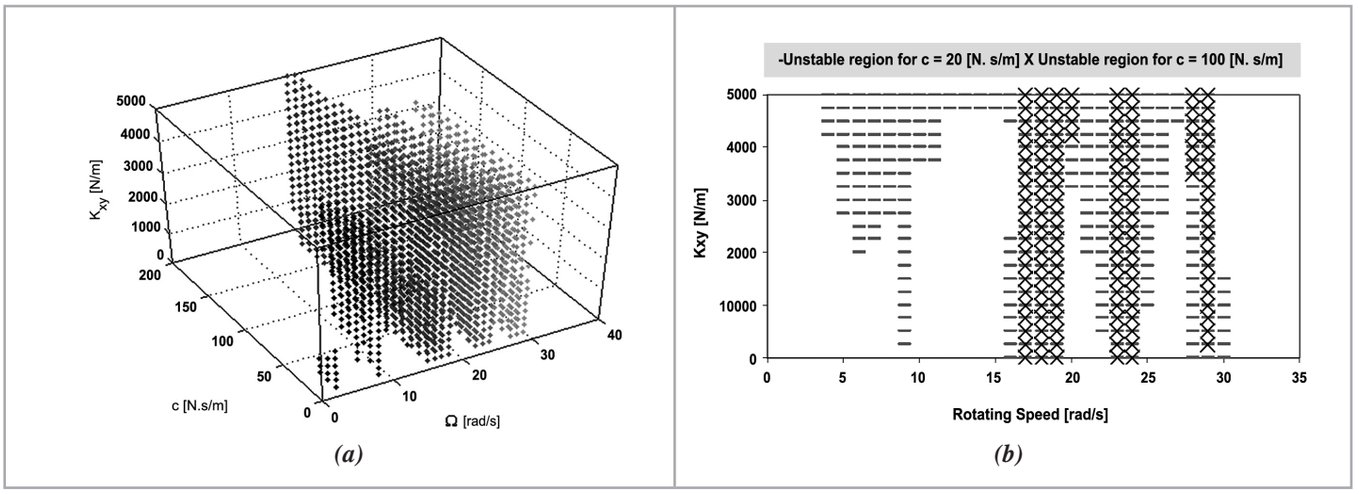

Figure 7: (a) Unstable region (dotted) as a function of external damping, cross-coefficient stiffness and rotating speed. (b) Influence of damping to unstable region.

6.0 CONCLUSIONS

Rotor dynamics subjected to parametric excitation are evaluated by means of Runge-Kutta method and Floquet theory. By comparing the results obtained using these two methods, it is found that the discrepancy is very low (approximately 1%).

Moreover, computation time and resources needed for evaluation of Hill's determinant is significantly more efficient than Runge-Kutta method. By inspection of whirl speed chart, the researcher can immediately have an idea of where the unstable speed region is. On the other hand, in order to produce instability region from Runge-Kutta method, one has to assess multiple time histories, which each of them is evaluated with different rotation speed, and this is very time consuming. However, the time history produced can be utilised to procure vibration frequencies using Fast Fourier Transform (FFT).

Although higher-order Hill's determinant produces better approximation and revealing higher order unstable regions, this comes with the expense of higher computational load. The recommended strategy is to start with first and second-order Hill's determinant. By determining the percentage improvement of the solutions, one can then assess the need to further evaluate solution of higher-order.

In addition, higher cross-coefficient stiffness of anisotropic support increases the overall unstable region. On the other hand, higher damping in supporting structure reduces unstable region. ■

REFERENCES

[1] Chapra S., and Canale R. (2003). Numerical Methods for Engineers, 4th Edition, Mcgraw-Hill, ISBN 0072431938.

[2] Ganesan, R. (2000). "Effects of bearing and shaft asymmetries on the instability of rotors operating at near-critical speeds." Mechanism and Machine Theory. 35: pp. 737-752.

[3] Iwatsubo, T., Tomita, A., and Kawai, R. (1973). "Vibrations of asymmetric rotors supported by asymmetric bearings." Archive of Applied Mechanics (Ingenieur Archiv). Springer, Berlin. 42(6): pp. 416-432.

[4] Kang, Y., Lee, and Y.-G., Chen, S.-C. (1997). "Instability analysis of unsymmetrical rotor-bearing systems using the transfer matrix method." Journal Sound and Vibration. 199(3): pp. 381-400.

[5] Lee, C.-W., Han, D.-J., Suh, J.-H., and Hong, S.-W. (2007). "Modal analysis of periodically time-varying linear rotor systems." Journal of Sound and Vibration. 303(3-5): pp. 553-574.

[6] Nayfeh A., and Mook D. (1979). Nonlinear Oscillations, John Wiley and Sons, ISBN 0471035556.

[7] Ota, H., and Mizutani, K. (1978). "Influence of unequal pedestal stiffness on the instability regions of a rotating asymmetric shaft." Transaction of the ASME, Journal of Applied Mechanics. 45: pp. 400-407.

[8] Parszeski, Z.A., Krodkiewski, J.M., and Rucinski, J. (1986). "Parametric instabilities of rotor-support systems with asymmetric stiffness and damping matrices." Journal of Sound and Vibration. 109(1): pp. 111-125.

[9] Rajalingham, C., Bhat, R.B., and Xistris, G.D. (1992). "Influence of support flexibility and damping characteristics on the stability of rotors with stiffness anisotropy about shaft principle axes." International Journal of Mechanical Sciences. 34(9): pp. 717-726.

[10] Tondl, A. (1965), Some Problems of Rotor Dynamics, Chapman and Hall, London.

PROFILES

LEE CHIH FENG
Lee Chih Feng is a postgraduate student at the University of Melbourne, Australia. He obtained B.Eng. (Hons) in Mechanical and Manufacturing Engineering from the same university in 2005. His research interests cover dynamics and automatic control.

TAN YEE WEI
Tan Yee Wei is an engineer involved in the field of water purification. He graduated from the University of Melbourne in 2005 with a B.Eng. (Hons) in mechanical engineering. His interests include modelling and simulation.

DR KRODKIEWSKI
After his graduation from the Technical University of Lodz in Poland, Dr Krodkiewski joined its Institute of Applied Mechanics in 1964. From the same University, in 1971, he obtained his doctorate in Mechanical Engineering. Since 1981 he has worked for the University of Melbourne and currently, as a senior fellow, is responsible for teaching Mechanics of Rigid Bodies, Dynamics of Machines and Dynamics of Rotors.